

Generative Multi-Label Zero-Shot Learning

Akshita Gupta*, Sanath Narayan*, Salman Khan, Fahad Shahbaz Khan, Ling Shao, Joost van de Weijer

Abstract—Multi-label zero-shot learning strives to classify images into multiple unseen categories for which no data is available during training. The test samples can additionally contain seen categories in the generalized variant. Existing approaches rely on learning either shared or label-specific attention from the seen classes. Nevertheless, computing reliable attention maps for unseen classes during inference in a multi-label setting is still a challenge. In contrast, state-of-the-art single-label generative adversarial network (GAN) based approaches learn to directly synthesize the class-specific visual features from the corresponding class attribute embeddings. However, synthesizing multi-label features from GANs is still unexplored in the context of zero-shot setting. When multiple objects occur jointly in a single image, a critical question is how to effectively fuse multi-class information. In this work, we introduce different fusion approaches at the attribute-level, feature-level and cross-level (across attribute and feature-levels) for synthesizing multi-label features from their corresponding multi-label class embeddings. To the best of our knowledge, our work is the first to tackle the problem of multi-label feature synthesis in the (generalized) zero-shot setting. Our cross-level fusion-based generative approach outperforms the state-of-the-art on three zero-shot benchmarks: NUS-WIDE, Open Images and MS COCO. Furthermore, we show the generalization capabilities of our fusion approach in the zero-shot detection task on MS COCO, achieving favorable performance against existing methods. Source code is available at https://github.com/akshita8/Generative_MLZSL

Index Terms—Generalized zero-shot learning, Multi-label classification, Zero-shot object detection, Feature synthesis

INTRODUCTION

MULTI-LABEL classification is a challenging problem where the task is to recognize all labels in an image. Typical examples of multi-label classification include, MS COCO [1] and NUS-WIDE [2] datasets, where an image may contain several different categories (labels). Most recent multi-label classification approaches address the problem by utilizing attention mechanisms [3, 4, 5], recurrent neural networks [6, 7, 8], graph CNNs [9, 10] and label correlations [11, 12]. However, these approaches do not tackle the problem of multi-label zero-shot classification, where the task is to classify images into multiple new “unseen” categories at test time, without being given any corresponding visual example during the training. Different from zero-shot learning (ZSL), the test samples can belong to the seen or unseen classes in generalized zero-shot learning (GZSL). Here, we tackle the challenging problem of large-scale multi-label ZSL and GZSL.

Existing multi-label (G)ZSL approaches address the problem by utilizing global image representations [13, 14], structured knowledge graphs [15] and attention-based mechanisms [16]. In contrast to the multi-label setting, single-label (generalized) zero-shot learning, where an image contains at most one category label, has received significant attention [17, 18, 19, 20, 21, 22, 23, 24, 25, 26]. State-of-the-art single-label (G)ZSL approaches [25, 26, 27, 28, 29, 30, 31] are generative in nature. These approaches exploit the power of generative models, such as generative adversarial networks (GANs) [32] and variational autoencoder (VAE) [33] to synthesize unseen class features. Typically, a feature synthesizing generator is utilized to construct single-label features. The generative approaches currently dominate single-label ZSL due to their ability to synthesize unseen

class (fake) features by learning the underlying data distribution of seen classes (real) features. Nevertheless, the generator only synthesizes single-label features in the existing ZSL frameworks. To the best of our knowledge, the problem of designing a feature synthesizing generator for *multi-label* ZSL paradigm is yet to be explored.

In this work, we address the problem of multi-label (generalized) zero-shot learning by introducing an approach based on the generative paradigm. When designing a generative multi-label zero-shot approach, the main objective is to synthesize semantically consistent *multi-label* visual features from their corresponding class attributes (embeddings). Multi-label visual features can be synthesized in two ways. (i) One approach is to integrate class-specific attribute embeddings at the input of the generator to produce a global image-level embedding vector. We call this approach attribute-level fusion (ALF). Here, the image-level embedding represents the holistic distribution of the positive labels in the image (see Fig. 1). Since the generator in ALF performs global image-level feature generation, it is able to better capture label dependencies (correlations among the labels) in an image. However, such a feature generation has lower class-specific discriminability since the discriminative information with respect to the individual classes is not explicitly encoded. (ii) A second approach is to synthesize the features from the class-specific embeddings individually and then integrate them in the visual feature space. We call this approach feature-level fusion (FLF), as shown in Fig. 1. Although FLF better preserves the class-specific discriminative information in the synthesized features, it does not explicitly encode the label dependencies in an image due to synthesizing features independently of each other. This motivates us to investigate an alternative fusion approach for multi-label feature synthesis.

In this work, we introduce an alternative fusion approach that combines the advantage of label dependency of ALF and the class-specific discriminability of FLF, during multi-label feature synthesis. We call this approach cross-level feature fusion (CLF), as in Fig. 1. The CLF approach utilizes each individual-level feature and attends to the bi-level context (from ALF and FLF). As a result, individual-level features adapt themselves to produce

- A. Gupta is with University of Guelph and Vector Institute. Correspondence to agupta22@uoguelph.ca
- S. Narayan is with Technology Innovation Institute, UAE.
- S. Khan and F. S. Khan. are with Mohamed Bin Zayed University of AI, UAE. S. Khan is also with Australian National University, Australia. F. S. Khan is also with Linköping University, Sweden.
- L. Shao is with the UCAS-Terminus AI Lab, University of Chinese Academy of Sciences, Beijing, China.
- J. van de Weijer is with Computer Vision Center, Universitat Autònoma de Barcelona, Spain.

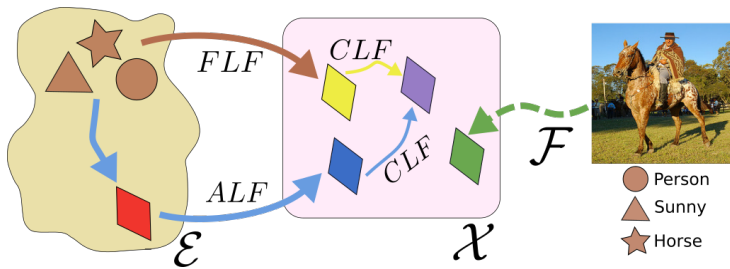


Fig. 1. A conceptual illustration of our three fusion approaches: attribute-level (ALF), feature-level (FLF) and cross-level feature (CLF), on an example image with three classes. Given an image, a feature extractor \mathcal{F} extracts real visual features (\blacklozenge) in \mathcal{X} . ALF integrates the individual class-specific embeddings to generate a global image-level embedding (\blacklozenge) in \mathcal{E} . The image-level embedding is then used to synthesize the multi-label features (\blacklozenge). Different from ALF, the FLF synthesizes class-specific features and integrates them in the feature space \mathcal{X} . These integrated features are shown as \blacklozenge . Our CLF takes as input synthesized features from ALF and FLF and enriches each respective feature by taking guidance from the other. The resulting enriched features are integrated to obtain the final image-level feature representation (\blacklozenge). The final image representation combines the advantage of label dependency of ALF and class-specific discriminability of FLF. The figure has been modified to include the color change suggested by the reviewers.

enriched synthesized features, which are then pooled to obtain the CLF output. In addition to multi-label zero-shot classification, we investigate the proposed multi-label feature generation CLF approach for (generalized) zero-shot object detection.

Contributions: We propose a generative approach for multi-label (generalized) zero-shot learning. To the best of our knowledge, we are the first to explore the problem of multi-label feature synthesis in the zero-shot setting. We investigate three different fusion approaches (ALF, FLF and CLF) to synthesize multi-label features. Our CLF approach combines the advantage of label dependency of ALF and the class-specific discriminability of FLF. Further, we integrate our fusion approaches into two representative generative architectures: \mathfrak{f} -CLSWGAN [25] and \mathfrak{f} -VAEGAN [26]. We hope our simple and effective method serves as a solid baseline and aids ease future research in generative *multi-label* zero-shot learning.

We evaluate our (generalized) zero-shot classification approach on NUS-WIDE [2], Open Images [34] and MS COCO [1]. Our CLF approach achieves consistent improvement in performance over both ALF and FLF. Furthermore, CLF outperforms state-of-the-art methods on *all* datasets. On the large-scale Open Images dataset, our CLF achieves absolute gains of 18.7% and 17.6% over the state-of-the-art in terms of GZSL F1 score at *top-K* predictions, $K \in \{10, 20\}$, respectively. We additionally evaluate CLF for (generalized) zero-shot object detection, achieving favorable results against existing methods on MS COCO.

2 GENERATIVE SINGLE-LABEL ZERO-SHOT LEARNING

As discussed earlier, state-of-the-art single-label zero-shot approaches [25, 26, 27, 28, 29, 30] are generative in nature, utilizing the power of generative models (*e.g.*, GAN [32], VAE [33]) to synthesize unseen class features. Here, each image is assumed to have a *single* object category label (*e.g.*, CUB [35], FLO [36] and AWA [24]).

Problem Formulation: Let $x \in \mathcal{X}$ denote the encoded feature instances of images and $y \in \mathcal{Y}^s$ the corresponding class labels from the set of S seen class labels $\mathcal{Y}^s = \{y_1, \dots, y_S\}$. Let $\mathcal{Y}^u = \{y_{S+1}, \dots, y_C\}$ denote the set of U unseen classes, which is disjoint from the seen classes \mathcal{Y}^s . Here, the total number of seen and unseen classes is denoted by $C=S+U$. The relationships among all the seen and unseen classes are described by the

category-specific semantic embeddings $e(k) \in \mathcal{E}$, $\forall k \in \mathcal{Y}^s \cup \mathcal{Y}^u$. To learn the ZSL and GZSL classifiers, existing single-label GAN-based approaches [25, 26, 28, 29] first learn a generator using the seen class features x_s and corresponding class embeddings $e(y_s)$. Then, the learned generator and the unseen class embeddings $e(y_u)$ are used to synthesize the unseen class features \tilde{x}_u . The resulting synthesized features \tilde{x}_u , along with the real seen class features x_s , are further deployed to train the final classifiers $f_z: \mathcal{X} \rightarrow \mathcal{Y}^U$ and $f_{gz}: \mathcal{X} \rightarrow \mathcal{Y}^C$.

Typically, GAN-based single-label zero-shot frameworks utilize a feature synthesizing generator $G: \mathcal{Z} \times \mathcal{E} \rightarrow \mathcal{X}$ and a discriminator D . Both G and D compete against each other in a two player minimax game. While D attempts to accurately distinguish real image features x from generated features \tilde{x} , G attempts to fool D by generating features that are semantically close to real features. Since class-specific features are to be synthesized, a conditional Wasserstein GAN [37] is employed due to its more stable training, by conditioning both G and D on the embeddings $e(y)$. Here, G learns to synthesize class-specific features \tilde{x} from the corresponding single-label embeddings $e(y)$, given by $\tilde{x} = G(z, e(y))$. Nevertheless, the generator only synthesizes single-label features in existing zero-shot learning frameworks. To the best of our knowledge, the problem of designing a feature synthesizing generator for the multi-label zero-shot learning paradigm is yet to be investigated.

3 GENERATIVE MULTI-LABEL ZERO-SHOT LEARNING

As discussed earlier, most real-world tasks involve multi-label recognition, where an image can contain multiple and wide range of category labels (*e.g.*, Open Images [34]). Multi-label classification becomes more challenging in the zero-shot learning setting, where the test set either contains only unseen classes (ZSL) or both seen and unseen classes (GZSL). In this work, we propose a generative multi-label zero-shot learning approach that exploits the capabilities of generative models to learn the underlying data distribution of seen classes. This helps to mimic the fully-supervised setting by synthesizing (fake) features for unseen classes. Different from the single-label setting, multi-label feature synthesis requires accurate integration of multi-class information regarding different objects jointly occurring in an image. Here, *multi-label* visual features representing different objects in an image need to be synthesized from a set of corresponding class embeddings. Thus, accurately fusing class information w.r.t each label embedding becomes critical in multi-label feature synthesis.

Problem Formulation: In contrast to single-label zero-shot learning, here, $x \in \mathcal{X}$ denotes the encoded feature instances of multi-label images and $y \in \{0, 1\}^S$ the corresponding multi-hot labels from the set of S seen class labels \mathcal{Y}^s . Let x denote the multi-label feature instance of an image and y , its multi-hot label with n positive classes in the image. Then, the set of attributes for the image can be denoted as $e(y) = \{e(y_j), \forall j: y[j]=1\}$, where $|e(y)|=n$. Here, we use GloVe [38] vectors of the class names as the attributes $e(y_j)$, as in [16]. Now, the generator's task is to learn to synthesize the multi-label features x from the associated embedding vectors $e(y)$. Post-training of G , multi-label features corresponding to the unseen classes are synthesized. The resulting synthesized features along with the real seen class features are deployed to train the final classifiers $f_z: \mathcal{X} \rightarrow \{0, 1\}^U$ and $f_{gz}: \mathcal{X} \rightarrow \{0, 1\}^C$.

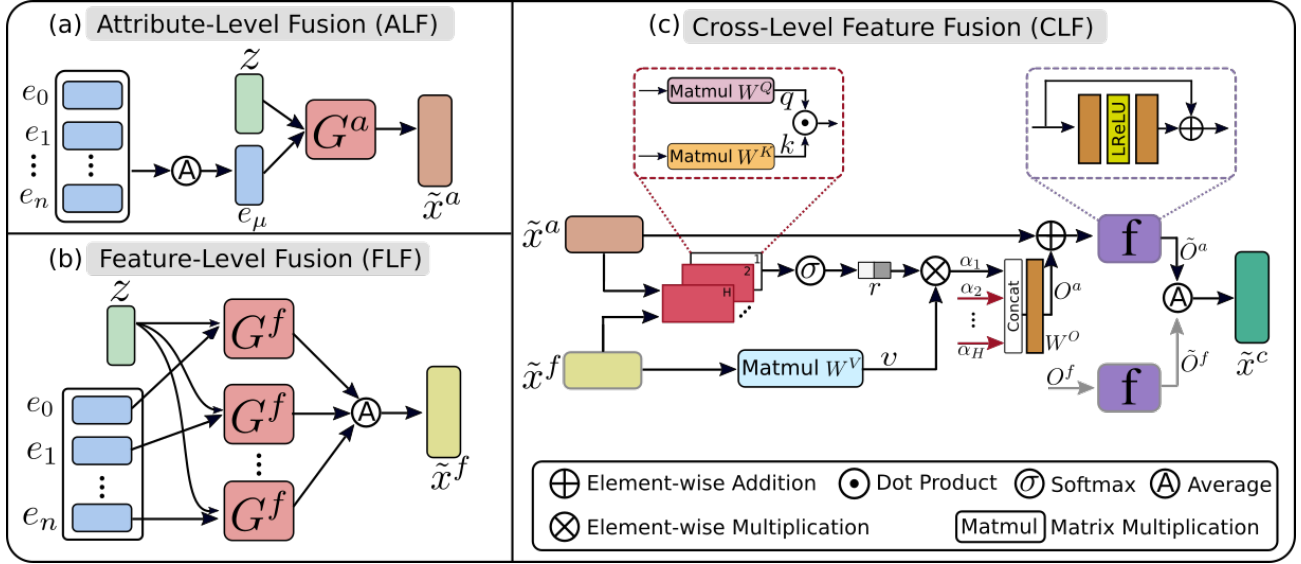


Fig. 2. Overview of three different approaches to synthesize unseen multi-label features. The attribute-level fusion (ALF) generates a global image-level embedding vector from a set of class-specific embedding vectors corresponding to multiple labels in an image (Sec. 3.1.1). In ALF, the generator synthesizes global features \tilde{x}^a that capture the correlations among the labels in the image. On the other hand, the feature-level fusion (FLF) synthesizes features from individual class-specific embeddings (Sec. 3.1.2). As a result, the generator produces class-specific latent features which are then integrated to obtain synthesized features \tilde{x}^f . The cross-level fusion (CLF) combines the advantages of ALF and FLF; during feature generation (Sec. 3.1.3). Specifically, it uses each individual-level feature (\tilde{x}^a, \tilde{x}^f) to attend to the bi-level context and adapt itself to generate \tilde{o}^a, \tilde{o}^f . These enriched features are then pooled to obtain the CLF output, which represents our final synthesized feature \tilde{x}^c .

3.1 Generative Multi-Label Feature Synthesis

To synthesize multi-label features, we introduce three fusion approaches: attribute-level fusion (ALF), feature-level fusion (FLF) and cross-level feature fusion (CLF).

3.1.1 Attribute-Level Fusion

In attribute-level fusion (ALF) approach, a global image-level embedding vector is obtained from a set of class-specific embedding vectors that correspond to multiple labels in the image. The image-level embedding represents the global description of the positive labels in an image. The global embedding e_μ is obtained by averaging the individual class embeddings $e(y)$. This embedding e_μ is then input to the generator G^a along with the noise z for synthesizing the feature \tilde{x}^a . The attribute-level fusion is then given by

$$e_\mu = \frac{1}{n} \sum_{j:y[j]=1} e(y_j) \quad \text{and} \quad \tilde{x}^a = G^a(z, e_\mu). \quad (1)$$

Fig. 2(a) shows the feature synthesis of \tilde{x}^a from the embedding e_μ . The generator G^a in ALF performs global image-level feature generation, thereby capturing label dependencies (correlations among labels) in an image. However, such a generation from the global embedding has lower class-specific discriminability since it does not explicitly encode discriminative information w.r.t individual classes.

3.1.2 Feature-Level Fusion

Here, we introduce a feature-level fusion (FLF) approach, which synthesizes the features from the class-specific embeddings individually. This allows the FLF approach to better preserve the class-specific discriminability in the synthesized features. Different from ALF that integrates the class embeddings, the FLF first inputs the n class-specific embeddings $e(y_j)$ to G^f and generates n class-specific latent features \tilde{x}_j . These features are then integrated through an average operation to obtain the final

synthesized feature \tilde{x}^f . The feature-level fusion (FLF) is denoted by

$$\tilde{x}_j = G^f(z, e(y_j)) \quad \text{and} \quad \tilde{x}^f = \frac{1}{n} \sum_{j:y[j]=1} \tilde{x}_j. \quad (2)$$

Fig. 2(b) shows the feature generation of \tilde{x}^f from the individual embeddings $e(y_j)$. We observe from Eq. 2 that for a fixed noise z , the generator G^f synthesizes a fixed latent feature \tilde{x}_j for class j , regardless of the presence/absence of other classes in an image. Thus, while the generated latent features \tilde{x}_j better preserve class-specific discriminative information of the positive classes j present in the image, G^f synthesizes them independently of each other. As a result, the synthesized feature \tilde{x}^f does not explicitly encode the label dependencies in an image.

As discussed above, both the aforementioned fusion approaches (ALF and FLF) have shortcomings when synthesizing multi-label features. Next, we introduce a fusion approach that combines the advantage of the label dependency of ALF and class-specific discriminability of FLF.

3.1.3 Cross-Level Feature Fusion

The proposed cross-level feature fusion (CLF) aims to combine the advantages of both ALF and FLF. The CLF approach (see Fig. 2(c)) incorporates label dependency and class-specific discriminability in the feature generation stage as in the ALF and FLF, respectively. To this end, \tilde{x}^f and \tilde{x}^a are forwarded to a feature fusion block. Inspired by the multi-headed self-attention [39], the feature fusion block enriches each respective feature by taking guidance from the other branch. Specifically, we create a matrix $\tilde{x} \in \mathbb{R}^{2 \times d}$ by stacking the individual features \tilde{x}^f and \tilde{x}^a . Then, these features are linearly projected to a low-dimensional space ($d' = d/H$) to create query-key-value triplets using a total of H projection heads,

$$q_h = \tilde{x}W_h^Q, k_h = \tilde{x}W_h^K, v_h = \tilde{x}W_h^V,$$

where $W_h^Q, W_h^K, W_h^V \in \mathbb{R}^{d \times d'}$ and $h \in \{1, 2, \dots, H\}$. For each feature, a status of its current form is kept in the 'value' embedding,

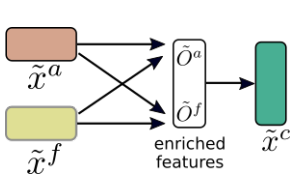


Fig. 3. Conceptual illustration showing the cross-level fusion mechanism. The multi-label feature \tilde{x}^a that is generated by ALF gets enriched by employing attention on itself and \tilde{x}^f from FLF. Similarly, \tilde{x}^f also gets enriched with the aid of \tilde{x}^a . The resulting enriched features \tilde{o}^a and \tilde{o}^f are then combined to obtain the final CLF feature \tilde{x}^c .

while the *query* vector derived from each input feature is used to find its correlation with the *keys* obtained from both the features, as we elaborate below.

Given these triplets from each head, the features undergo two levels of processing (i) intra-head processing on the triplet and (ii) cross-head processing. For the first case, the following equation is used to relate each query vector with ‘keys’ derived from both the features. The resulting normalized relation scores ($r_h \in \mathbb{R}^{2 \times 2}$) from the softmax function (σ) are used to reweight the corresponding value vectors, thereby obtaining the attended features $\alpha_h \in \mathbb{R}^{2 \times d'}$,

$$\alpha_h = r_h v_h, \quad \text{where } r_h = \sigma\left(\frac{q_h k_h^\top}{\sqrt{d'}}\right).$$

To aggregate information across all heads, these attended low-dimensional features from each head are concatenated and processed by an output layer to generate the original d -dimensional output vectors $o \in \mathbb{R}^{2 \times d}$,

$$o = [\alpha_1; \alpha_2; \dots; \alpha_H] W^O, \quad (3)$$

where $W^O \in \mathbb{R}^{d \times d}$ is a learnable weight matrix. After obtaining the self-attended features o , a residual branch is added from the input to the attended features and further processed with a small residual sub-network $f(\cdot)$ to help the network first focus on the local neighbourhood and then progressively pay attention to the other-level features,

$$\tilde{o} = f(\tilde{x} + o) + (\tilde{x} + o), \quad \text{s.t.}, \tilde{o} \in \mathbb{R}^{2 \times d}. \quad (4)$$

This encourages the network to selectively focus on adding complimentary information to the source vectors \tilde{x} . Finally, we mean-pool the matrix \tilde{o} along the row dimension to obtain a single cross-level fused feature $\tilde{x}^c \in \mathbb{R}^d$,

$$\tilde{x}^c = \frac{1}{2} \sum_{j \in \{1,2\}} \tilde{o}^{j,k}. \quad (5)$$

The cross-level fused feature \tilde{x}^c is obtained by effectively fusing the features generated from ALF and FLF (see Fig. 3). As a result, \tilde{x}^c explicitly encodes the correlation among labels in the image, in addition to the class-specific discriminative information of the positive classes present. Next, we describe the integration of our CLF in representative generative architectures for multi-label zero-shot classification.

3.2 Multi-Label Zero-Shot Classification

We integrate our fusion approaches in two representative generative architectures (f -CLSWGAN [25] and f -VAEGAN [26]) for multi-label zero-shot classification. Both f -CLSWGAN and f -VAEGAN have been shown to achieve promising performance for single-label zero-shot classification. Since CLF integrates both ALF and FLF, we only describe here the integration of CLF in the two classification frameworks. Next, we describe the integration of CLF in f -CLSWGAN, followed by f -VAEGAN.

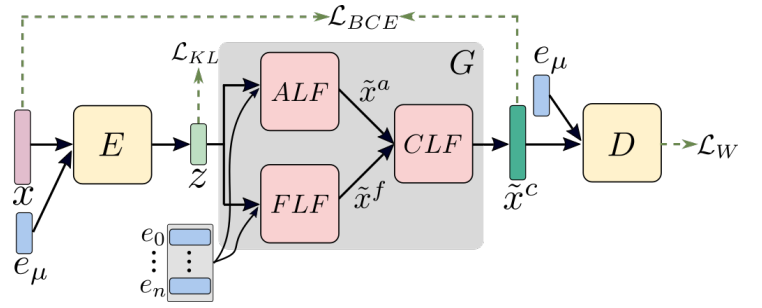


Fig. 4. Our CLF-based f -VAEGAN architecture, which integrates the proposed multi-label feature synthesis CLF approach into the f -VAEGAN. The standard f -VAEGAN extends f -CLSWGAN by integrating a conditional VAE along with a conditional WGAN, utilizing a shared generator between them. f -VAEGAN comprises an encoder E , shared generator and a discriminator D , conditioned on the class-specific embeddings e . In the proposed CLF-based f -VAEGAN shown here, we replace the single-label shared generator in f -VAEGAN with our multi-label generator G for synthesizing multi-label \tilde{x}^c . The resulting synthesized features \tilde{x}^c are then passed to the discriminator for training the generator using the loss terms: \mathcal{L}_{KL} , \mathcal{L}_{BCE} and \mathcal{L}_W .

Briefly, f -CLSWGAN comprises a WGAN, conditioned on the embeddings $e(y)$, and a seen class classifier f_{cls} . We replace the standard generator of f -CLSWGAN with our multi-label feature generator (CLF) to synthesize multi-label features \tilde{x}^c . The resulting multi-label WGAN loss is,

$$\mathcal{L}_W = \mathbb{E}[D(x_s, e(y_s))] - \mathbb{E}[D(\tilde{x}_s^c, e(y_s))] - \lambda \mathbb{E}[(\|\nabla_{\hat{x}} D(\hat{x}, e(y_s))\|_2 - 1)^2], \quad (6)$$

where \tilde{x}_s^c is synthesized using Eq. 5 for the seen classes, λ is the penalty coefficient and \hat{x} is a convex combination of x_s and \tilde{x}_s^c . Furthermore, a classifier f_{cls} , trained on the seen classes, is employed to encourage the generator to synthesize features that are well suited for final ZSL/GZSL classification. The final objective for training our CLF-based f -CLSWGAN in a multi-label setting is given by,

$$\min_G \max_D \mathcal{L}_W + \alpha \mathbb{E}[\text{BCE}(f_{cls}(\tilde{x}_s^c), y_s)], \quad (7)$$

where $\text{BCE}(f_{cls}(\tilde{x}_s^c), y_s)$ denotes the standard binary cross entropy loss between the predicted multi-label $f_{cls}(\tilde{x}_s^c)$ and the ground-truth multi-label y_s of feature x_s .

In addition to f -CLSWGAN, we also integrate our CLF into f -VAEGAN [26] framework to perform multi-label feature synthesis. The f -VAEGAN extends f -CLSWGAN by combining a conditional VAE [33] along with a conditional WGAN, utilizing a shared generator between them. For more details on f -VAEGAN, we refer to [26]. Similar to our CLF-based f -CLSWGAN described earlier, we replace the single-label shared generator in f -VAEGAN with our multi-label generator (CLF) for synthesizing multi-label \tilde{x}^c . The resulting CLF-based f -VAEGAN is trained similar to the standard f -VAEGAN, using the original loss formulation [26]. Fig.4 shows our CLF-based f -VAEGAN architecture for multi-label (generalized) zero-shot classification.

4 EXPERIMENTS

Datasets: We evaluate our approach on three benchmarks: NUS-WIDE [2], Open Images [34] and MS COCO [1]. The **NUS-WIDE** dataset comprises nearly 270K images with 81 human-annotated categories, in addition to the 925 labels obtained from Flickr user tags. As in [14, 16], the 925 and 81 labels are used as seen and unseen classes, respectively. The **Open Images** (v4) is a large-scale dataset with 9 million training images along with 41,620 validation and 125,456 testing images. It is partially annotated

with human and machine-generated labels. Here, 7,186 labels, with at least 100 training images, are selected as seen classes. The most frequent 400 test labels, which are not present in the training data are selected as unseen classes, as in [16]. The MS COCO dataset is divided into training and validation sets with 82,783 and 40,504 images. Here, we perform multi-label zero-shot experiments by using the same split (65 seen and 15 unseen classes), as in [40, 41].

Evaluation Metrics: Similar to [16, 42], we evaluate our zero-shot classification approach using the F1 score at *top-K* predictions and the mean Average Precision (mAP). While the F1 captures the model’s ability to correctly rank the labels in each image, the mAP metric captures the image ranking accuracy of the model for each label.

Multi-label Combinations: Synthesizing multi-label features for learning the final multi-label ZSL and GZSL classifiers requires multi-label combinations with only unseen classes and also seen-unseen classes. To obtain these combinations, first, given a multi-label combination of seen classes from the training set, we randomly change the seen classes to their corresponding nearest unseen classes (based on distance between the class embeddings in the word-embedding space \mathcal{E}). This allows us to obtain different multi-label combinations involving only unseen classes and seen-unseen classes. Consequently, our approach aids in the obtaining multi-label combinations that are more likely to be realistic and occurring in the test distribution.

Implementation Details: Following existing zero-shot classification works [14, 16], we use the pretrained VGG-19 backbone to extract features from multi-label images. Image-level features of size $d=4,096$ from FC7 layer output are used as input to our GAN. We use the l_2 normalized 300 dimensional GloVe [38] vectors corresponding to the category names as the embeddings $e(k) \in \mathcal{E}$, as in [16]. The encoder E , discriminator D and generators G^a and G^f are two layer fully connected (FC) networks with 4,096 hidden units and Leaky ReLU non-linearity. The number of heads H in our CLF is set to 8. The sub-network $f(\cdot)$ in CLF is a two layer FC network with 8,192 hidden units. The feature synthesizing network is trained with a 10^{-4} learning rate. The WGAN is trained with (*batch size*, *epoch*) of (64, 50), (128, 1) and (64, 70) on NUS-WIDE, Open Images and MS COCO, respectively. For the f -CLSWGAN variant, α is set to 0.1, while λ is set to 10 in the f -VAEGAN variant. The ZSL and GZSL classifiers: f_z and f_{gz} are trained for 50 epochs with (*batch size*, *learning rate*) of (300, 10^{-3}), (100, 10^{-4}) and (100, 10^{-3}) on NUS-WIDE, Open Images and MS COCO, respectively. We use the ADAM optimizer with (β_1 , β_2) as (0.5, 0.999) for training. All the parameters are chosen via cross-validation.

4.1 Ablation Study

We first present an ablation study w.r.t our fusion approaches: attribute-level (ALF), feature-level (FLF) and cross-level feature (CLF) on the NUS-WIDE dataset. We evaluate our fusion strategies with both architectures: f -CLSWGAN and f -VAEGAN. Tab. 1 shows the comparison, in terms of F1 score ($K \in \{3, 5\}$) and mAP for both ZSL and GZSL tasks. In the case of ZSL, the ALF-based f -CLSWGAN achieves mAP score of 22.1. The FLF-based f -CLSWGAN obtains similar performance with mAP score of 22.6. The CLF-based f -CLSWGAN achieves improved performance with mAP score of 23.7. Similarly, the CLF-based f -CLSWGAN obtains consistent improvement over both ALF and FLF-based f -CLSWGAN in terms of F1 score ($K \in \{3, 5\}$). In the case of GZSL, ALF and FLF obtain F1 scores ($K=3$) of 16.8 and 17.0, respectively. Our CLF approach achieves improved performance

TABLE 1

Classification performance comparison of the three fusion approaches (ALF, FLF and CLF) for both ZSL and GZSL tasks on the NUS-WIDE dataset. The comparison is shown in terms of F1 score ($K \in \{3, 5\}$) and mAP. We present the evaluation of our fusion approaches with both architectures: f -CLSWGAN and f -VAEGAN. Regardless of the underlying generative architecture, our CLF approach achieves consistent improvement in performance, on all metrics, over both ALF and FLF for ZSL and GZSL tasks. Best results are in bold.

Fusion	GAN	Task	F1 (K=3)	F1 (K=5)	mAP
ALF	f -CLSWGAN	ZSL	29.8	26.7	22.1
		GZSL	16.8	19.7	7.1
	f -VAEGAN	ZSL	30.9	27.9	22.9
		GZSL	17.7	20.6	7.5
FLF	f -CLSWGAN	ZSL	29.8	26.8	22.6
		GZSL	17.0	19.6	7.2
	f -VAEGAN	ZSL	29.9	27.0	23.3
		GZSL	17.2	19.9	7.6
CLF	f -CLSWGAN	ZSL	31.1	27.6	23.7
		GZSL	17.9	20.7	8.0
	f -VAEGAN	ZSL	32.8	29.3	25.7
		GZSL	18.9	22.0	8.9

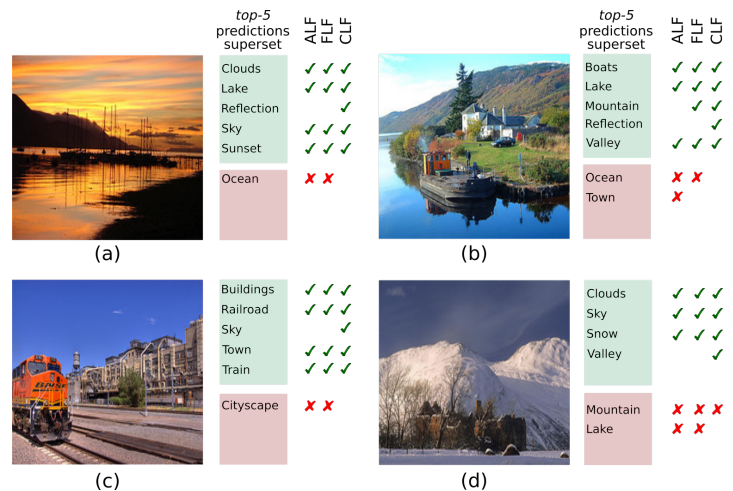


Fig. 5. Qualitative results for the ZSL task on examples from NUS-WIDE. Alongside each example is a superset of *top-5* predictions from our ALF, FLF and CLF. The true- and false-positive classes are enclosed in green and red boxes. For each fusion approach, a green tick (✓) and a red cross (✗) is shown for true- and false-positive labels in its *top-5* predictions, respectively. Labels absent in the *top-5* predictions of a fusion have no ✓ or ✗. Our CLF, which integrates ALF and FLF, provides superior classification performance by correctly predicting classes missed by ALF and FLF, e.g., *Reflection* in (a) and *Sky* in (c), while removing false predictions such as, *Ocean* in (b) and *Lake* in (d).

with F1 score of 17.9. Similarly, CLF performs favorably against both ALF and FLF in terms of F1 at $K=5$ and mAP metrics.

As in f -CLSWGAN, we also observe the CLF approach to achieve consistent improvement in performance over both ALF and FLF, when integrated in the more sophisticated f -VAEGAN. In the case of ZSL, our CLF-based f -VAEGAN achieves absolute gains of 2.8% and 2.4% in terms of mAP over ALF and FLF, respectively. Similarly, CLF-based f -VAEGAN achieves consistent improvement in performance in terms of F1 score, over both ALF and FLF. Furthermore, CLF-based f -VAEGAN performs favorably against the other two fusion approaches in case of GZSL. Fig. 5 shows example qualitative results demonstrating the favorable performance of CLF over ALF and FLF. Additional qualitative results are illustrated in Sec. 6.

The aforementioned results show that our CLF approach achieves consistent improvement in performance over both ALF

TABLE 2

State-of-the-art comparison for ZSL and GZSL tasks on the NUS-WIDE and Open Images datasets. For a fair comparison, we use the same dataset splits (seen/unseen classes) as in LESA [16]. We report the results in terms of mAP and F1 score at $K \in \{3, 5\}$ for NUS-WIDE and $K \in \{10, 20\}$ for Open Images. Our approach outperforms the state-of-the-art for both ZSL and GZSL tasks, in terms of mAP and F1 score, on both datasets. Best results are in bold.

Method	Task	NUS-WIDE (#seen / #unseen = 925/81)						Open Images (#seen / #unseen = 7186/400)							
		K = 3			K = 5			mAP	K = 10			K = 20			mAP
		P	R	F1	P	R	F1		P	R	F1	P	R	F1	
CONSE [43]	ZSL	17.5	28.0	21.6	13.9	37.0	20.2	9.4	0.2	7.3	0.4	0.2	11.3	0.3	40.4
	GZSL	11.5	5.1	7.0	9.6	7.1	8.1	2.1	2.4	2.8	2.6	1.7	3.9	2.4	66.1
LabelEM [23]	ZSL	15.6	25.0	19.2	13.4	35.7	19.5	7.1	0.2	8.7	0.5	0.2	15.8	0.4	40.5
	GZSL	15.5	6.8	9.5	13.4	9.8	11.3	2.2	4.8	5.6	5.2	3.7	8.5	5.1	68.7
Fast0Tag [14]	ZSL	22.6	36.2	27.8	18.2	48.4	26.4	15.1	0.3	12.6	0.7	0.3	21.3	0.6	41.2
	GZSL	18.8	8.3	11.5	15.9	11.7	13.5	3.7	14.8	17.3	16.0	9.3	21.5	12.9	68.6
One Attention per Label [44]	ZS	20.9	33.5	25.8	16.2	43.2	23.6	10.4	-	-	-	-	-	-	-
	GZSL	17.9	7.9	10.9	15.6	11.5	13.2	3.7	-	-	-	-	-	-	-
One Attention per Cluster (M=10) [16]	ZSL	20.0	31.9	24.6	15.7	41.9	22.9	12.9	0.6	22.9	1.2	0.4	32.4	0.9	40.7
	GZSL	10.4	4.6	6.4	9.1	6.7	7.7	2.6	15.7	18.3	16.9	9.6	22.4	13.5	68.2
LESA (M=10) [16]	ZSL	25.7	41.1	31.6	19.7	52.5	28.7	19.4	0.7	25.6	1.4	0.5	37.4	1.0	41.7
	GZSL	23.6	10.4	14.4	19.8	14.6	16.8	5.6	16.2	18.9	17.4	10.2	23.9	14.3	69.0
Our Approach	ZSL	26.6	42.8	32.8	20.1	53.6	29.3	25.7	1.3	42.4	2.5	1.1	52.1	2.2	43.0
	GZSL	30.9	13.6	18.9	26.0	19.1	22.0	8.9	33.6	38.9	36.1	22.8	52.8	31.9	75.5

TABLE 3

(G)ZSL performance comparison, on NUS-WIDE, between using (i) random combinations of classes for synthesizing multi-label features and (ii) our approach of obtaining seen-unseen combinations from the train set multi-label combinations by replacing random seen classes with their nearest unseen classes. We observe that learning the final ZSL and GZSL classifiers with features of multi-label combinations obtained by our approach significantly improves the zero-shot classification performance in comparison to learning with random multi-label combinations, which are likely to synthesize unrealistic features.

Method	Task	F1 (K=3)	F1 (K=5)	mAP
Random	ZSL	28.0	26.1	21.0
	GZSL	15.8	17.9	6.1
Ours	ZSL	32.8	29.3	25.7
	GZSL	18.9	22.0	8.9

and FLF for both ZSL and GZSL, regardless of the underlying architecture. Moreover, the best results are obtained when integrating our CLF in f -VAEGAN. Unless stated otherwise, we refer to our CLF-based f -VAEGAN as “Our Approach” from here on.

Varying the Multi-label Combinations for Feature Synthesis:

Here, we conduct an experiment to analyze the effect of generating unrealistic images from completely random multi-label combinations and report the results in Tab. 3. We observe that using random combinations decreases the multi-label classification performance in comparison to our approach of replacing a seen class with its nearest unseen class. Specifically, for the ZSL task, our approach obtains gains of 4.8, 3.2 and 4.7 in terms of F1 ($K=3$), F1 ($K=5$) and mAP, respectively, in comparison to employing random multi-label features. We also observe a similar trend in the case of GZSL task.

Varying the Fusion: Here, we compare our cross-level feature fusion (CLF) with two fusion baselines: (i) averaging the output of ALF and FLF; (ii) concatenating the output of ALF and FLF, followed by an MLP. The results tabulated in Tab. 4 show that the our CLF approach achieves significant gains over both AVG and CONCAT on both ZSL and GZSL tasks.

Varying the Backbone: Here, we experiment with image features extracted from different backbones and report the results in Tab. 5. We observe that using stronger backbones improves the classification performance for both ZSL and GZSL tasks. *E.g.*, employing a ResNet-50 pretrained in a self-supervised manner

TABLE 4

(G)ZSL performance comparison of our CLF approach with baseline fusion approaches such as average (AVG) and concatenation (CONCAT) on the NUS-WIDE dataset, in terms of F1 and mAP. We observe that our cross-level feature fusion (CLF) approach achieves significant gains over both the baselines on both (G)ZSL tasks.

Fusion	Task	F1 (K=3)	F1 (K=5)	mAP
AVG	ZSL	30.2	27.4	23.2
	GZSL	17.4	20.1	7.5
CONCAT	ZSL	30.5	27.8	23.6
	GZSL	17.8	20.6	7.7
Ours: CLF	ZSL	32.8	29.3	25.7
	GZSL	18.9	22.0	8.9

TABLE 5

(G)ZSL performance comparison of our CLF approach on the NUS-WIDE dataset, when employing different backbones. We observe that the performance of our CLF for both (G)ZSL tasks improves when using stronger backbones like DINO ResNet-50 [45].

Backbone	Task	F1 (K=3)	F1 (K=5)	mAP
VGG [46]	ZSL	32.8	29.3	25.7
	GZSL	18.9	22.0	8.9
Places365 ResNet-50 [47]	ZSL	33.0	29.9	26.0
	GZSL	19.2	22.4	9.3
DINO ResNet-50 [45]	ZSL	33.7	30.7	27.1
	GZSL	20.1	23.2	10.4

(DINO [45]) improves the mAP by 1.4 and 1.5 for the ZSL and GZSL tasks. Furthermore, unless otherwise stated, we employ VGG as the backbone to enable a fair comparison with existing multi-label zero-shot approaches [14, 16].

4.2 State-of-the-art Comparison

NUS-WIDE: Tab. 2 shows the state-of-the-art comparison¹ for zero-shot (ZSL) and generalized zero-shot (GZSL) classification. The results are reported in terms of mAP and F1 score at *top-K* predictions ($K \in \{3, 5\}$). In addition, we also report the precision (P) and recall (R) for each F1 score. For the ZSL

1. We exclude [48, 49] from quantitative comparison due to the differences in training setup and evaluation metric computation.

TABLE 6

State-of-the-art comparison for ZSL and GZSL tasks on the MS COCO dataset having 65 seen and 15 unseen classes. We report the results in terms of mAP and F1 score at $K=3$ for ZSL and $K=\{3, 5\}$ for GZSL. Our approach performs favorably against existing approaches for both ZSL and GZSL tasks. Best results are in bold.

Method	Task	F1 (K=3)	F1 (K=5)	mAP
CONSE [43]	ZSL	18.4	-	13.2
	GZSL	19.6	18.9	7.7
LabelEM [23]	ZSL	10.3	-	9.6
	GZSL	6.7	7.9	4.0
Fast0tag [14]	ZSL	37.5	-	43.3
	GZSL	33.8	34.6	27.9
LESA [16]	ZSL	33.6	-	31.8
	GZSL	26.7	28.0	17.5
Our Approach	ZSL	43.5	-	52.2
	GZSL	44.1	43.4	33.2

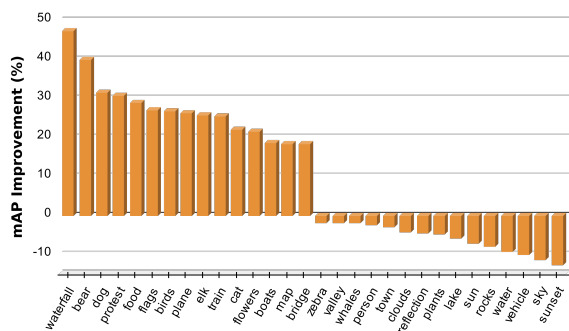


Fig. 6. Classification mAP improvement comparison between our approach and LESA on NUS-WIDE. We show the comparison for 15 unseen labels with the largest gain as well 15 unseen labels with the largest drop. Our approach significantly improves (more than 26%) on several unseen labels (e.g., *waterfall*, *bear*, *dog*, *protest* and *food*), while having relatively smaller (less than 12%) negative impact on other labels. Best viewed zoomed in.

task, Fast0Tag [14], which finds principal directions in the word vector space for ranking the relevant tags ahead of irrelevant tags, achieves an mAP of 15.1. The recently introduced LESA [16], utilizing shared multi-attention to predict all labels in an image, achieves improved results over Fast0Tag, with an mAP of 19.4. Our approach sets a new state of the art, outperforming LESA with an absolute gain of 6.3% in terms of mAP. Similarly, our approach obtains consistent improvement in performance over the state-of-the-art in terms of F1 score ($K \in \{3, 5\}$). For the GZSL task, LESA obtains improved classification results among existing methods with an mAP of 5.6. Our approach achieves mAP score of 8.9, outperforming LESA with an absolute gain of 3.3%. Similarly, our approach achieves consistent improvement in performance with absolute gains of 4.5% and 5.2% over LESA in terms of F1 score at $K=3$ and $K=5$, respectively.

Fig. 6 shows the classification comparison of our approach w.r.t LESA for 15 unseen labels with the largest performance gain as well as 15 unseen labels with the largest drop. Our approach significantly improves (more than 26%) on several labels, such as *waterfall*, *bear*, *dog*, *protest* and *food*, while having relatively smaller (less than 12%) negative impact on labels, such as *sunset*, *person*, *sky*, *water* and *rocks*. We observe our approach to be particularly better on animal classes (11 out of 13). In total, our approach outperforms LESA on 57 out of 81 labels.

Open Images: Tab. 2 shows the state-of-the-art comparison for ZSL and GZSL tasks. The results are reported in terms of mAP and F1 score at $top-K$ predictions ($K \in \{10, 20\}$). Since only 4,728

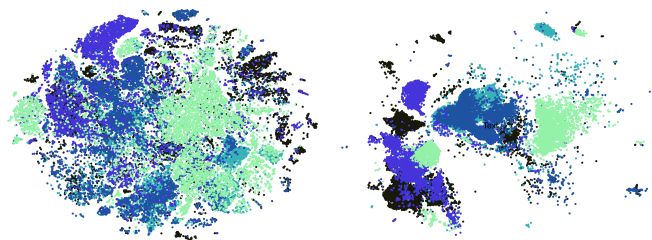


Fig. 7. Qualitative comparison, in terms of t-SNE plots, between a recent discriminative approach BiAM [50] (on the left) and our CLF employed on top of BiAM (on the right). Visual feature instances from $top-5$ frequently occurring unseen classes in the test set of the NUS-WIDE dataset are utilized for obtaining the t-SNE plots. The plots show that the features of different classes are better separated (and thereby discriminative) in the case of BiAM+CLF (on the right) compared to the class features from BiAM alone (on the left).

seen classes are present in the testing set instances, the mAP score for the GZSL task is obtained by averaging AP for the 5,128 (seen+unseen) classes, following [34]. Compared to NUS-WIDE, Open Images has significantly larger number of labels. This makes the ranking problem within an image more challenging, reflected by the lower F1 scores in the table. For the ZSL task, LESA obtains F1 scores of 1.4 and 1.0 at $K=10$ and $K=20$, respectively. Our approach performs favorably against LESA with F1 scores of 2.5 and 2.2 at $K=10$ and $K=20$, respectively. A similar performance gain is also observed for the mAP metric. It is worth noting that this dataset has 400 unseen labels, thereby making the problem of ZSL challenging. As in ZSL, our approach also achieves consistent gains, in both F1 and mAP, over the state-of-the-art for GZSL.

MS COCO: We are the first to evaluate zero-shot classification on this dataset. Tab. 6 shows the state-of-the-art comparison for ZSL and GZSL tasks. Since the maximum number of unseen classes per image is 3 in *val* set, we report the F1 at only $K=3$ for the ZSL task. We re-implement LabelEM, CONSE and Fast0tag since the respective source codes are not publicly available. For LESA, we obtain the results using the code-base provided by the authors. Our approach obtains superior (G)ZSL performance, in both F1 score and mAP, compared to existing methods. Particularly, our approach obtains significant gains of 8.9% and 5.3% in terms of mAP for the ZSL and GZSL tasks over Fast0Tag [14]. Similar gains over the existing methods are also obtained for F1 score on both tasks, showing the efficacy of our approach.

Impact of Employing CLF with Discriminative Approaches:

Here, we conduct an experiment for analyzing the effect of improved discriminability of the synthesized multi-label unseen class features. To this end, we employ the recent discriminative multi-label ZSL approaches LESA [16] and BiAM [50] as multi-label feature extractors and learn our CLF on these features. Tab. 8 shows that the ZSL and GZSL classification performance improves when employing our fusion-based CLF on top of these recent approaches. This is likely due to the discriminative approaches being trained on the seen class multi-label features alone and thereby relying on the mapping in the visual-semantic joint space for classifying novel unseen classes. However, in our CLF approach, zero-shot classifiers have better knowledge of the unseen classes since they are learned using the synthesized unseen class features. Furthermore, in Fig. 7, t-SNE plots show the improvement in unseen class feature discriminability when CLF is learned on the BiAM features [50].

TABLE 7

State-of-the-art comparison for ZSL and GZSL tasks on the NUS-WIDE and Open Images datasets *using the proposed splits*. We report the results in terms of mAP and F1 score at $K \in \{3, 5\}$ for NUS-WIDE. Similarly, F1 score for Open Images is computed at $K \in \{3, 5\}$ for ZSL and $K \in \{10, 20\}$ for GZSL. Our approach outperforms the state-of-the-art for both ZSL and GZSL tasks, in terms of mAP and F1 score, on both datasets. Best results are in bold.

Method	Task	NUS-WIDE (#seen / #unseen = 837/84)						mAP	Open Images (#seen / #unseen = 7186/367)						mAP
		K = 3			K = 5				K = 3 (ZSL), 10 (GZSL)			K = 5 (ZSL), 20 (GZSL)			
		P	R	F1	P	R	F1		P	R	F1	P	R	F1	
Fast0Tag [14]	ZSL	20.1	23.3	21.6	17.4	33.6	22.9	13.9	2.6	3.1	2.8	2.9	9.6	4.5	62.1
	GZSL	24.6	10.9	15.2	20.1	14.9	17.1	5.1	16.9	19.9	18.2	10.2	23.5	14.2	66.8
LESA (M=10) [16]	ZSL	21.0	24.3	22.5	18.1	34.9	23.8	14.2	3.2	7.8	4.5	3.2	12.7	5.1	62.3
	GZSL	29.0	12.9	17.8	23.6	17.5	20.1	6.5	18.3	21.1	19.6	11.2	25.8	15.6	67.2
Our Approach	ZSL	22.7	26.2	24.3	19.3	37.2	25.6	16.1	3.5	11.5	5.4	4.3	14.5	6.5	64.5
	GZSL	30.2	13.5	18.6	25.2	18.8	21.4	9.5	33.6	38.8	36.0	22.7	52.8	31.8	75.3

TABLE 8

Impact of employing our CLF on top of recent discriminative approaches (LESA [16] and BiAM [50]). The performance of our CLF is also reported for ease of comparison. We observe that replacing the VGG backbone feature extractor in our CLF with LESA and BiAM significantly improves the performance in terms of F1 and mAP for (G)ZSL tasks over the respective discriminative approaches. These results show that our generative CLF approach can be easily integrated with state-of-the-art discriminative approaches to improve the multi-label zero-shot classification performance.

Method	Task	F1 (K=3)	F1 (K=5)	mAP
CLF	ZSL	32.8	29.3	25.7
	GZSL	18.9	22.0	8.9
LESA [16]	ZSL	31.6	28.7	19.4
	GZSL	14.4	16.8	5.6
LESA [16] + CLF	ZSL	36.6	32.7	27.9
	GZSL	20.4	23.1	8.2
BiAM [50]	ZSL	33.1	30.7	26.3
	GZSL	16.1	19.0	9.3
BiAM [50] + CLF	ZSL	38.5	35.1	29.4
	GZSL	23.2	25.3	10.2

4.3 State-of-the-art Comparison on Proposed Splits

The seen/unseen class splits [14, 16] for NUS-WIDE and Open Images employed by existing approaches for evaluating on the multi-label (G)ZSL tasks do not strictly conform with the zero-shot paradigm. This is because the backbones used for feature extraction are pre-trained on the ImageNet [51] dataset, whose classes overlap with a few unseen classes of NUS-WIDE and Open Images. Note that this issue does not arise for the MS COCO experiments since the backbone is retrained after removing the overlapping ImageNet classes, as in [41]. Thus, in order to conform with the ZSL paradigm, we propose new seen/unseen splits for both NUS-WIDE and Open Images by ensuring that there is no overlap between the pre-trained ImageNet classes and the new unseen classes of the respective datasets.

NUS-WIDE: We first preprocess the data to remove any label inconsistencies. In the original split of 925/81, there were multiple pairs with identical classes but minor spelling variations, e.g., *harbor-harbour*, *window-windows*, *animal-animals*. Such classes in each pair are merged and considered as a single class in the proposed split. Furthermore, classes originally in unseen set but overlapping with ImageNet classes are moved to the seen class set. Similarly, a few seen classes that had no overlap with ImageNet classes are moved to the unseen set to balance the splits. Consequently, the proposed (G)ZSL split for NUS-WIDE contains 837 seen classes and 84 unseen classes.

Open Images: The original 400 unseen classes are present only in the test set and do not have any corresponding annotation in the 5.5 million training images. Hence, only the unseen classes that overlap with the ImageNet classes are removed and not

TABLE 9

Standard multi-label classification performance comparison on NUS-WIDE. The results are reported in terms of mAP and F1 score at $K \in \{3, 5\}$. Our approach achieves superior performance compared to existing methods. Best results are in bold.

Method	K=3			K=5			mAP
	P	R	F1	P	R	F1	
Logistic [52]	46.1	57.3	51.1	34.2	70.8	46.1	21.6
WARP [53]	49.1	61.0	54.4	36.6	75.9	49.4	3.1
WSABIE [11]	48.5	60.4	53.8	36.5	75.6	49.2	3.1
Fast0Tag [14]	48.6	60.4	53.8	36.0	74.6	48.6	22.4
CNN-RNN [6]	49.9	61.7	55.2	37.7	78.1	50.8	28.3
One Attention per Label [44]	51.3	63.7	56.8	38.0	78.8	51.3	32.6
One Attention per Cluster [16]	51.1	63.5	56.6	37.6	77.9	50.7	31.7
LESA [16]	52.3	65.1	58.0	38.6	80.0	52.0	31.5
Our Approach	53.5	66.5	59.3	39.4	81.6	53.1	46.7

considered during evaluation. This results in 367 unseen classes being retained in the proposed split. Furthermore, following [16], testing instances without any unseen class annotations are not considered when evaluating for the ZSL task. In addition, since nearly 95% and 99% of the testing images have less than 3 and 5 unseen classes, respectively, we compute the F1 scores at $K \in \{3, 5\}$ for the ZSL task. However, we retain $K \in \{10, 20\}$ for GZSL, as in [16]. Further details regarding the classes in the proposed splits for both datasets are provided in the appendix.

Tab. 7 shows the performance comparison of our method with existing approaches (Fast0Tag [14] and LESA [16]) on the proposed splits of NUS-WIDE and Open Images. Our approach performs favorably in comparison to existing methods, achieving significant gains over LESA up to 3% and 8.1% for NUS-WIDE and Open Images, in terms of mAP on the GZSL task. Similar gains for F1 scores are also achieved by our approach for both ZSL and GZSL. These results reinforce that *irrespective of the seen/unseen class splits*, our approach performs favorably against existing methods on both ZSL and GZSL tasks in the multi-label setting.

4.4 Standard Multi-Label Classification

In addition to zero-shot classification, we evaluate our approach for standard multi-label classification where all the category labels during training and testing are identical. Tab. 9 shows the state-of-the-art comparison on NUS-WIDE with 81 human annotated labels. As in [16], we remove all the testing instances that do not have any classes corresponding to the 81 labels set. Among the existing methods, CNN-RNN and LESA achieve mAP scores of 28.3 and 31.5, respectively. Our approach outperforms existing methods by achieving an mAP score of 46.7. Our

TABLE 10

Standard multi-label classification performance comparison on Open Images. The results are reported in terms of mAP and F1 score at $K \in \{10, 20\}$. Our approach achieves superior performance compared to existing methods. Best results are in bold.

Method	K=10			K=20			mAP
	P	R	F1	P	R	F1	
Logistic [52]	12.1	14.7	13.3	8.4	20.2	11.8	75.1
WARP [53]	7.1	8.5	7.7	5.3	12.6	7.4	69.9
WSABIE [11]	1.5	3.7	2.2	1.5	3.7	2.2	71.7
Fast0Tag [14]	14.9	17.9	16.2	9.3	22.3	13.1	69.0
CNN-RNN [6]	8.7	10.5	9.6	5.4	13.1	10.5	62.3
One Attention per Cluster [16]	14.9	17.9	16.3	9.2	22.0	13.0	68.5
LESA [16]	16.2	19.6	17.8	10.3	24.7	14.5	69.3
Our Approach	34.0	40.7	37.0	23.3	54.9	32.7	76.9

method also performs favorably against these methods in terms of F1 scores.

Similarly, we also evaluate on the large-scale Open Images dataset [34]. Tab. 10 shows the state-of-the-art comparison for the standard multi-label classification on Open Images, with 7,186 classes used for training and evaluating the approaches. As in [16], test samples with missing labels for these 7,186 classes are removed during evaluation. Furthermore, since only 4,728 ground-truth classes are present in the test set, following [34], the mAP score is obtained as the mean of AP for these classes only. Among the existing methods, Fast0Tag [14] and LESA [16] achieve an F1 score of 13.1 and 14.5 at $K=20$. Our approach outperforms the existing approaches by achieving an F1 score of 32.7. The proposed approach also performs favorably in comparison to existing methods in terms of mAP score. Consequently, these performance gains over existing methods on both datasets for the standard multi-label classification task show the efficacy of our approach.

5 EXTENSION TO ZERO-SHOT OBJECT DETECTION

Lastly, we also evaluate our multi-label feature generation approach (CLF) for zero-shot object detection (ZSD). ZSD strives for simultaneous classification and localization of previously unseen objects. In the generalized settings, the test set contains both seen and unseen object categories (GZSD). Recently, the work of [41] introduce a zero-shot detection approach (SUZOD) where features are synthesized, conditioned upon class-embeddings, and integrated in the popular Faster R-CNN framework [54]. The feature generation stage is jointly driven by the classification loss in the semantic embedding space for both seen and unseen categories. Their approach addresses multi-label zero-shot detection by constructing single-label features for each region of interest (RoI). Different from SUZOD [41], we first generate a pool of multi-label RoI features by integrating random sets of individual single-label RoI features.

To generate multi-label features for training our multi-label feature generation (CLF) approach, we first obtain the single-label features for foreground and background regions from the training images, as in SUZOD [41]. These single-label features are taken from the output of *ROI Align* layer in the Faster R-CNN framework [54] and correspond to a single proposal obtained from the region proposal network (RPN). The foreground RoI-aligned seen class features of an image are then randomly combined to generate multiple multi-label features. These multi-label features are then passed through the two-layer fully connected

TABLE 11

State-of-the-art comparison for ZSD and GZSD tasks on MS COCO. The results are reported in terms of mean Average Precision (mAP) and Recall (Rec). For GZSD, we report the harmonic mean (HM) between seen and unseen classes. Our approach performs favorably against existing methods. Best results are in bold.

Metric	Method	Seen/Unseen Split	ZSD	GZSD		
				Seen	Unseen	HM
mAP	SB [40]	48/17	0.70	-	-	-
	DSES [40]	48/17	0.54	-	-	-
	PL-48 [55]	48/17	10.01	35.92	4.12	7.39
	PL-65 [55]	65/15	12.40	34.07	12.40	18.18
	SUZOD [41]	65/15	19.00	36.90	19.00	25.08
	Our Approach	65/15	20.30	37.60	20.30	26.36
Rec	SB [40]	48/17	24.39	-	-	-
	DSES [40]	48/17	27.19	15.02	15.32	15.17
	PL-48 [55]	48/17	43.56	38.24	26.32	31.18
	PL-65 [55]	65/15	37.72	36.38	37.16	36.76
	SUZOD [41]	65/15	54.40	57.70	54.40	55.74
	Our Approach	65/15	58.10	58.90	58.10	58.50

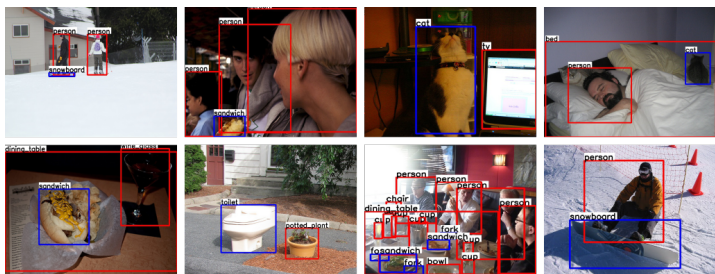


Fig. 8. Qualitative detection results for GZSD on example images from MS COCO using our multi-label CLF-based detection approach. The seen and unseen class detections are shown in red and blue. Our detection approach achieves promising detection performance for both seen and unseen classes.

network that follows the *ROI Align* layer in the Faster R-CNN, to obtain 1024-d multi-label features. The resulting seen class RoI features are then used as real features for training our multi-label feature generation (CLF) approach. Post-training of CLF, single-label unseen class features are synthesized and used for training the classifier for unseen classes. The learned classifier is then combined with the classifier head of the Faster R-CNN, as in SUZOD [41]. Query images with unseen classes are then input to the modified Faster R-CNN framework to obtain detections for the unseen classes.

Tab. 11 shows the state-of-the-art comparison, in terms of mAP and recall, for ZSD and GZSD detection on MS COCO. For GZSD, Harmonic Mean (HM) of performances for seen and unseen classes are reported. Similar to SUZOD [41], we also report the results by using f -CLSWGAN as the underlying generative architecture. The polarity loss approach (PL-65) [55] achieves an mAP of 12.4 for the ZSD task, while the single-label feature generating approach of SUZOD [41] achieves an improved performance of 19.0 mAP. Our approach performs favorably against SUZOD with a significant gain of 1.3% in terms of mAP. Furthermore, while PL-65 [55] achieves a recall score of 37.72 for ZSD, the SUZOD method [41] achieves a recall of 54.4. Our CLF-based multi-label feature generative approach performs favorably in comparison to existing methods by achieving a recall score of 58.1 for ZSD. Similarly, our approach also achieves consistent improvements for GZSD in terms of both mAP and recall. Fig. 8 shows qualitative detection results for GZSD. These results show that our approach improves the detection of unseen objects in (generalized) zero-shot settings.

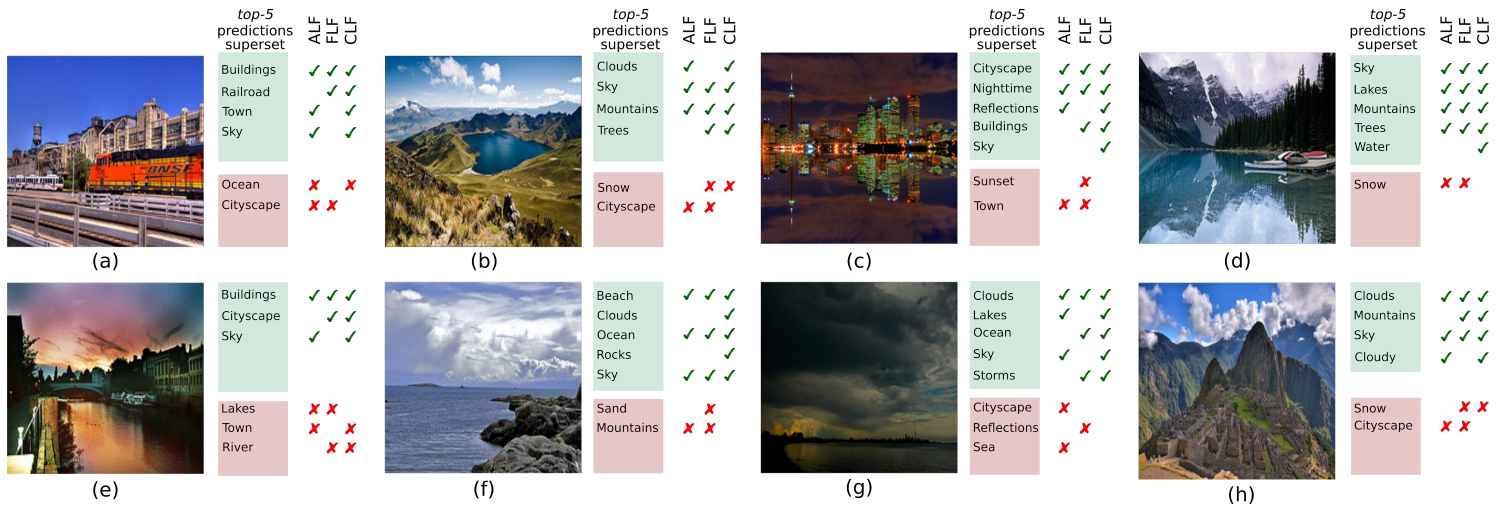


Fig. 9. Qualitative results for multi-label ZSL on eight example images from the NUS-WIDE dataset. Alongside each example image is a superset of *top-5* predictions from our three fusion approaches: attribute-level (ALF), feature-level (FLF) and cross-level feature fusion (CLF). The true positive classes are enclosed in a green box. Similarly, false positives are enclosed in a red box. A green tick (✓) is shown for a fusion approach if it has predicted the corresponding true positive label in its *top-5* predictions. Similarly, a red cross (✗) is shown for a false-positive label in its *top-5* predictions. A label without a tick or cross for a fusion approach denotes that its absence in the *top-5* predictions. Generally, our ALF and FLF approaches predict the true positives reasonably well. Our CLF, which integrates ALF and FLF approaches, improves the classification further with increased true positives and reduced false positives. Our CLF approach correctly predicts classes that were missed by both ALF and FLF, e.g., *Sky* in image (c) and *Water* in image (d). Furthermore, our CLF removes the false predictions of *Town* and *Snow* in (c) and (d), respectively. In addition, classes such as *Mountains* in (h) and *Reflections* in (c) are predicted correctly by either ALF or FLF, while both labels are correctly predicted by CLF. A similar observation holds in image (g). These results show that our CLF combines the advantages of both ALF and FLF, resulting in improved performance.

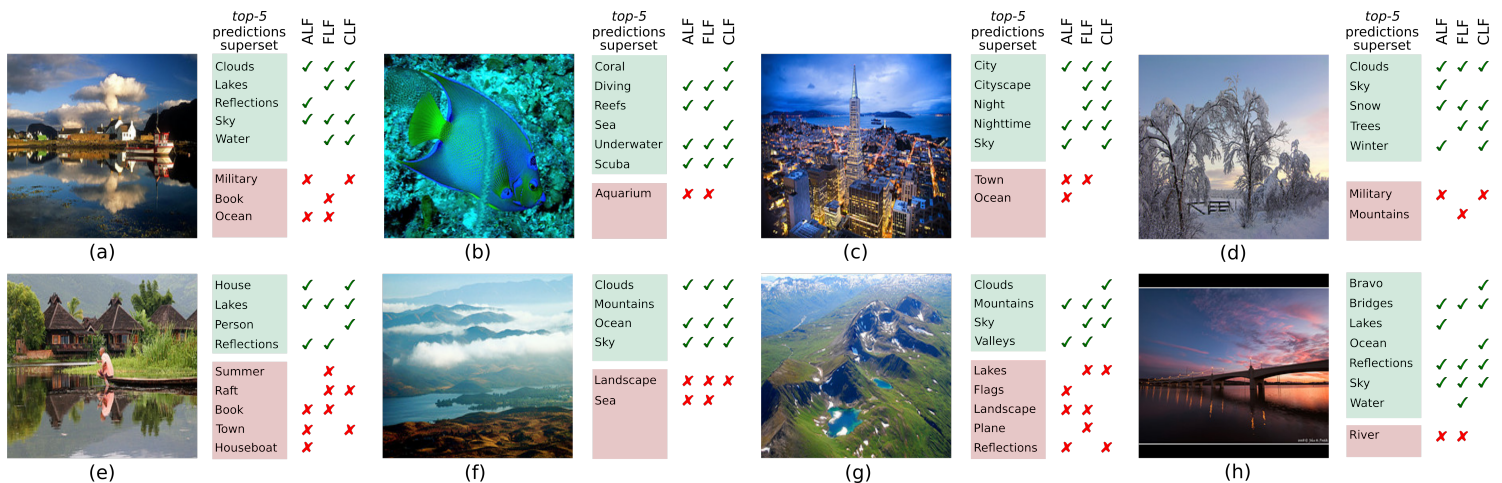


Fig. 10. Qualitative results for multi-label GZSL on eight example images from the NUS-WIDE dataset. While our ALF and FLF approaches predict the true positives to a reasonable extent, our CLF improves the classification further with increased true positives and reduced false positives. Our CLF approach correctly predicts classes that were missed by both ALF and FLF, e.g., *Coral*, *Sea* in image (b) and *Mountains* in image (f). False positives such as *Ocean* and *Aquarium* in (a) and (b) are also removed by our CLF. Furthermore, our CLF also correctly predicts classes such as *Cityscape*, *Sky* and *Night* in image (c), which were predicted by either ALF or FLF. These results show that our CLF, which integrates our ALF and FLF approaches, achieves consistent improvement in performance over both ALF and FLF. See also Fig. 9 for more details.

6 ADDITIONAL QUALITATIVE RESULTS

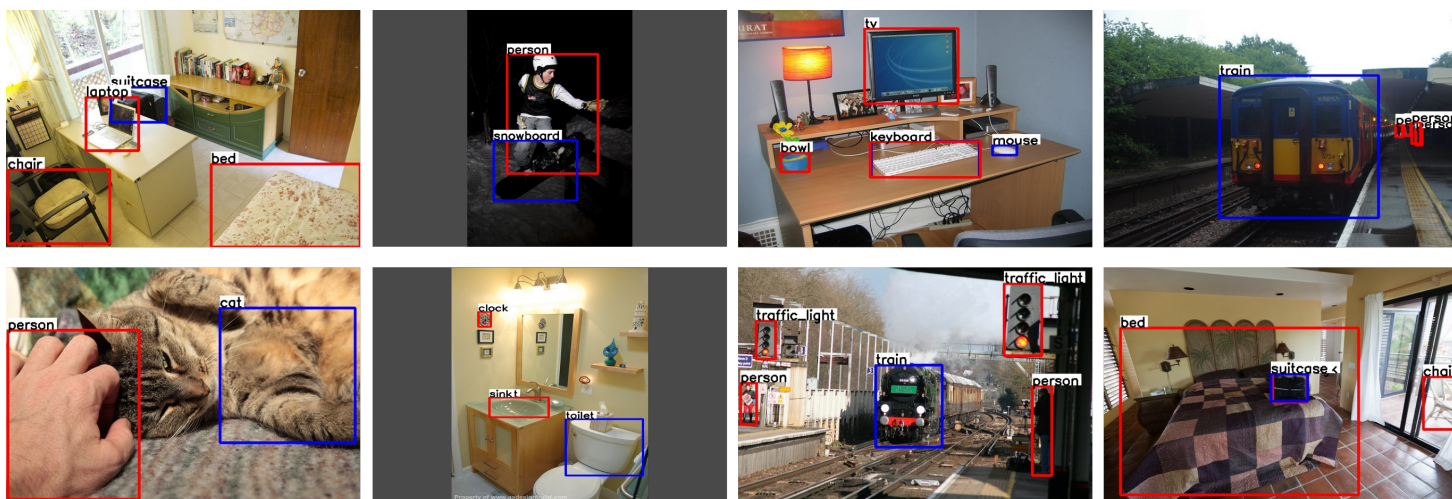
Multi-Label Zero-Shot Classification: Additional qualitative results are shown for multi-label zero-shot learning (ZSL) and generalized zero-shot learning (GZSL) in Fig. 9 and 10, respectively. Each figure comprises nine example images from the test set of the NUS-WIDE dataset [2]. Alongside each example image is a list with the superset of *top-5* predictions from our three fusion approaches: attribute-level (ALF), feature-level (FLF) and cross-level feature fusion (CLF). The true positives, i.e., prediction labels matching the ground-truth classes in the image, are enclosed in a green box. Similarly, false positives, i.e., prediction labels that do not match with the ground-truth classes are enclosed in a red box. A green tick (✓) is shown for a fusion approach if it has predicted the corresponding true positive label in its *top-5*

top-5 predictions. Similarly, a red cross (✗) is shown for a fusion approach if it has predicted the corresponding false-positive label in its *top-5* predictions. A label without a tick or cross for a fusion approach denotes its absence in the *top-5* predictions.

In general, we observe that our ALF and FLF approaches predict true positives reasonably well in their *top-5* predictions. Furthermore, our CLF approach, which combines the advantages of both ALF and CLF, increases the true positives and reduces the false positives, leading to consistent performance gains over both ALF and FLF. Our CLF approach correctly predicts classes missed by both ALF and FLF, e.g., *Sky* in Fig. 9(c), *Clouds* in Fig. 9(f), *Coral* in Fig. 10(b) and *Mountains* in Fig. 10(f). Moreover, our CLF also removes false positives such as *Snow* in Fig. 9(d) and *Town* in Fig. 10(c). In addition, our CLF correctly predicts



(a) Zero-shot object detection (ZSD)



(b) Generalized zero-shot object detection (GZSD)

Fig. 11. Qualitative results for zero-shot object detection on example images from the MS COCO dataset using our CLF approach. The zero-shot setting is illustrated in (a) followed by the generalized zero-shot setting in (b). The unseen classes detections are shown in blue, while the seen class predictions are in red. The unseen classes, such as *snowboard*, *airplane*, *train* and *cat* are correctly detected under zero-shot setting in (a), though the visual examples of these classes were not available for training. Similarly, we see that both unseen and seen classes are detected accurately under generalized zero-shot setting (b). These results show that our multi-label feature generation approach (CLF) achieves reasonably accurate object detection in (generalized) zero-shot settings.

classes such as *Railroad* in Fig. 9(a), *Lakes* in Fig. 9(g), *Cityscape*, *Sky* and *Night* in Fig. 10(c), which were predicted by either ALF or FLF. These results show the efficacy of our CLF approach that integrates our ALF and FLF, leading to improved (generalized) zero-shot classification.

Zero-Shot Object Detection: Fig. 11 shows additional qualitative results of our CLF approach on example images from the MS COCO dataset [1] for the zero-shot object detection task. The zero-shot setting with only unseen classes detected is shown in Fig. 11(a), followed by the generalized zero-shot setting in Fig. 11(b), where both unseen and seen classes are detected. While the unseen classes detections are denoted by blue bounding boxes, the seen class detections are shown in red. We observe that the unseen classes, such as *snowboard*, *airplane*, *train* and *cat* are correctly detected under zero-shot setting in Fig. 11(a), though the visual examples of these classes were not available for training. Furthermore, in the generalized zero-shot setting in Fig. 11(b), we see that both unseen and seen classes are also detected accurately. These results show that our multi-label feature generation approach (CLF) achieves reasonably accurate

object detection in (generalized) zero-shot settings.

In summary, our multi-label feature generation (CLF) approach, which integrates our attribute-level and feature-level fusion approaches, performs favorably in comparison to existing approaches on various tasks including (generalized) zero-shot multi-label classification, standard multi-label classification and (generalized) zero-shot detection.

7 CONCLUSION

We investigate the problem of multi-label feature synthesis in the zero-shot setting. To this end, we introduce three fusion approaches: ALF, FLF and CLF. Our ALF synthesizes features by integrating class-specific attribute embeddings at the generator input. The FLF synthesizes features from class-specific embeddings individually and integrates them in feature space. Our CLF combines the advantages of both ALF and FLF, using each individual-level feature and attends to the bi-level context. Consequently, individual-level features adapt themselves producing enriched synthesized features that are pooled to obtain the final

output. We integrate our fusion approaches in two generative architectures. Our approach outperforms existing zero-shot methods on three benchmarks. Additionally, our approach performs favorably against existing methods for the standard multi-label classification task on two large-scale benchmarks. Lastly, we also show the effectiveness of our approach for zero-shot detection. We hope our simple and effective approach will serve as a solid baseline and help ease future research in generative multi-label zero-shot learning.

8 ACKNOWLEDGMENT

The authors would like to acknowledge the support from Grant PID2021-128178OB-I00.

REFERENCES

- [1] T.-Y. Lin, M. Maire, S. Belongie, J. Hays, P. Perona, D. Ramanan, P. Dollár, and C. L. Zitnick, "Microsoft coco: Common objects in context," in *European Conference on Computer Vision*, 2014. 1, 2, 4, 11
- [2] T.-S. Chua, J. Tang, R. Hong, H. Li, Z. Luo, and Y. Zheng, "Nus-wide: a real-world web image database from national university of singapore," in *Conference On Image And Video Retrieval*, 2009. 1, 2, 4, 10, 14
- [3] Z. Wang, T. Chen, G. Li, R. Xu, and L. Lin, "Multi-label image recognition by recurrently discovering attentional regions," in *Proceedings of the IEEE/CVF International Conference on Computer Vision*, 2017. 1
- [4] J. Ye, J. He, X. Peng, W. Wu, and Y. Qiao, "Attention-driven dynamic graph convolutional network for multi-label image recognition," in *European Conference on Computer Vision*, 2020. 1
- [5] R. You, Z. Guo, L. Cui, X. Long, Y. Bao, and S. Wen, "Cross-modality attention with semantic graph embedding for multi-label classification," in *Proceedings of the AAAI Conference on Artificial Intelligence*, 2020. 1
- [6] J. Wang, Y. Yang, J. Mao, Z. Huang, C. Huang, and W. Xu, "Cnn-rnn: A unified framework for multi-label image classification," in *Proceedings of the IEEE/CVF Conference on Computer Vision and Pattern Recognition*, 2016. 1, 8, 9
- [7] V. O. Yazici, A. Gonzalez-Garcia, A. Ramisa, B. Twardowski, and J. v. d. Weijer, "Orderless recurrent models for multi-label classification," in *Proceedings of the IEEE/CVF Conference on Computer Vision and Pattern Recognition*, 2020. 1
- [8] J. Nam, E. Loza Mencía, H. J. Kim, and J. Fürnkranz, "Maximizing subset accuracy with recurrent neural networks in multi-label classification," *Advances in Neural Information Processing Systems*, 2017. 1
- [9] T. N. Kipf and M. Welling, "Semi-supervised classification with graph convolutional networks," *arXiv preprint arXiv:1609.02907*, 2016. 1
- [10] Z.-M. Chen, X.-S. Wei, P. Wang, and Y. Guo, "Multi-label image recognition with graph convolutional networks," in *Proceedings of the IEEE/CVF Conference on Computer Vision and Pattern Recognition*, 2019. 1
- [11] J. Weston, S. Bengio, and N. Usunier, "Wsabie: Scaling up to large vocabulary image annotation," in *International Journal of Computer Vision*, 2011. 1, 8, 9
- [12] T. Durand, N. Mehrasa, and G. Mori, "Learning a deep convnet for multi-label classification with partial labels," in *Proceedings of the IEEE/CVF Conference on Computer Vision and Pattern Recognition*, 2019. 1
- [13] T. Mensink, E. Gavves, and C. G. Snoek, "Costa: Co-occurrence statistics for zero-shot classification," in *Proceedings of the IEEE/CVF Conference on Computer Vision and Pattern Recognition*, 2014. 1
- [14] Y. Zhang, B. Gong, and M. Shah, "Fast zero-shot image tagging," in *Proceedings of the IEEE/CVF Conference on Computer Vision and Pattern Recognition*, 2016. 1, 4, 5, 6, 7, 8, 9
- [15] C.-W. Lee, W. Fang, C.-K. Yeh, and Y.-C. Frank Wang, "Multi-label zero-shot learning with structured knowledge graphs," in *Proceedings of the IEEE/CVF Conference on Computer Vision and Pattern Recognition*, 2018. 1
- [16] D. Huynh and E. Elhamifar, "A shared multi-attention framework for multi-label zero-shot learning," in *Proceedings of the IEEE/CVF Conference on Computer Vision and Pattern Recognition*, 2020. 1, 2, 4, 5, 6, 7, 8, 9
- [17] D. Jayaraman and K. Grauman, "Zero-shot recognition with unreliable attributes," in *Advances in Neural Information Processing Systems*, 2014. 1
- [18] Y. Fu, T. M. Hospedales, T. Xiang, and S. Gong, "Transductive multi-view zero-shot learning," *IEEE Transactions on Pattern Analysis and Machine Intelligence*, 2015. 1
- [19] A. Frome, G. S. Corrado, J. Shlens, S. Bengio, J. Dean, M. Ranzato, and T. Mikolov, "Devise: A deep visual-semantic embedding model," in *Advances in Neural Information Processing Systems*, 2013. 1
- [20] B. Romera-Paredes and P. Torr, "An embarrassingly simple approach to zero-shot learning," in *International Conference on Machine Learning*, 2015. 1
- [21] M. Rohrbach, S. Ebert, and B. Schiele, "Transfer learning in a transductive setting," in *Advances in Neural Information Processing Systems*, 2013. 1
- [22] M. Ye and Y. Guo, "Zero-shot classification with discriminative semantic representation learning," in *Proceedings of the IEEE/CVF Conference on Computer Vision and Pattern Recognition*, 2017. 1
- [23] Z. Akata, F. Perronnin, Z. Harchaoui, and C. Schmid, "Label-embedding for image classification," *IEEE Transactions on Pattern Analysis and Machine Intelligence*, 2015. 1, 6, 7
- [24] Y. Xian, C. H. Lampert, B. Schiele, and Z. Akata, "Zero-shot learning—a comprehensive evaluation of the good, the bad and the ugly," *IEEE Transactions on Pattern Analysis and Machine Intelligence*, 2018. 1, 2
- [25] Y. Xian, T. Lorenz, B. Schiele, and Z. Akata, "Feature generating networks for zero-shot learning," in *Proceedings of the IEEE/CVF Conference on Computer Vision and Pattern Recognition*, 2018. 1, 2, 4
- [26] Y. Xian, S. Sharma, B. Schiele, and Z. Akata, "f-vaegan-d2: A feature generating framework for any-shot learning," in *Proceedings of the IEEE/CVF Conference on Computer Vision and Pattern Recognition*, 2019. 1, 2, 4
- [27] R. Felix, B. G. V. Kumar, I. Reid, and G. Carneiro, "Multi-modal cycle-consistent generalized zero-shot learning," in *European Conference on Computer Vision*, 2018. 1, 2
- [28] J. Li, M. Jing, K. Lu, Z. Ding, L. Zhu, and Z. Huang, "Leveraging the invariant side of generative zero-shot learning," in *Proceedings of the IEEE/CVF Conference on Computer Vision and Pattern Recognition*, 2019. 1, 2
- [29] H. Huang, C. Wang, P. S. Yu, and C.-D. Wang, "Generative dual adversarial network for generalized zero-shot learning," in *Proceedings of the IEEE/CVF Conference on Computer Vision and Pattern Recognition*, 2019. 1, 2
- [30] D. Mandal, S. Narayan, S. K. Dwivedi, V. Gupta, S. Ahmed, F. S. Khan, and L. Shao, "Out-of-distribution detection for generalized zero-shot action recognition," in *Proceedings of the IEEE/CVF Conference on Computer Vision and Pattern Recognition*, 2019. 1, 2
- [31] S. Narayan, A. Gupta, F. S. Khan, C. G. Snoek, and L. Shao, "Latent embedding feedback and discriminative features for zero-shot classification," *arXiv preprint arXiv:2003.07833*, 2020. 1
- [32] I. Goodfellow, J. Pouget-Abadie, M. Mirza, B. Xu, and D. Warde-Farley, "Generative adversarial nets," in *Advances in Neural Information Processing Systems*, 2014. 1, 2
- [33] D. P. Kingma and M. Welling, "Auto-encoding variational bayes," *International Conference on Learning Representations*, 2014. 1, 2, 4
- [34] A. Kuznetsova, H. Rom, N. Alldrin, J. Uijlings, I. Krasin, J. Pont-Tuset, S. Kamali, S. Popov, M. Mallocci, T. Duerig *et al.*, "The open images dataset v4: Unified image classification, object detection, and visual relationship detection at scale," *arXiv preprint arXiv:1811.00982*, 2018. 2, 4, 7, 9, 14
- [35] P. Welinder, S. Branson, T. Mita, C. Wah, F. Schroff, S. Belongie,

- and P. Perona, "Caltech-ucsd birds 200," *Technical Report CNS-TR-2010-001, Caltech*, 2010. 2
- [36] M.-E. Nilsback and A. Zisserman, "Automated flower classification over a large number of classes," in *Indian Conference on Computer Vision, Graphics and Image Processing*, 2008. 2
- [37] M. Arjovsky, S. Chintala, and L. Bottou, "Wasserstein gan," *arXiv preprint arXiv:1701.07875*, 2017. 2
- [38] J. Pennington, R. Socher, and C. D. Manning, "Glove: Global vectors for word representation," in *Proceedings of the 2014 conference on empirical methods in natural language processing (EMNLP)*, 2014. 2, 5
- [39] A. Vaswani, N. Shazeer, N. Parmar, J. Uszkoreit, L. Jones, A. N. Gomez, Ł. Kaiser, and I. Polosukhin, "Attention is all you need," in *Advances in Neural Information Processing Systems*, 2017. 3
- [40] A. Bansal, K. Sikka, G. Sharma, R. Chellappa, and A. Divakaran, "Zero-shot object detection," in *European Conference on Computer Vision*, 2018. 5, 9
- [41] N. Hayat, M. Hayat, S. Rahman, S. Khan, S. W. Zamir, and F. S. Khan, "Synthesizing the unseen for zero-shot object detection," in *Proceedings of the Asian Conference on Computer Vision*, 2020. 5, 8, 9
- [42] A. Veit, N. Alldrin, G. Chechik, I. Krasin, A. Gupta, and S. Belongie, "Learning from noisy large-scale datasets with minimal supervision," in *Proceedings of the IEEE/CVF Conference on Computer Vision and Pattern Recognition*, 2017. 5
- [43] M. Norouzi, T. Mikolov, S. Bengio, Y. Singer, J. Shlens, A. Frome, G. S. Corrado, and J. Dean, "Zero-shot learning by convex combination of semantic embeddings," *arXiv preprint arXiv:1312.5650*, 2013. 6, 7
- [44] J.-H. Kim, J. Jun, and B.-T. Zhang, "Bilinear attention networks," in *Advances in Neural Information Processing Systems*, 2018. 6, 8
- [45] M. Caron, H. Touvron, I. Misra, H. Jégou, J. Mairal, P. Bojanowski, and A. Joulin, "Emerging properties in self-supervised vision transformers," in *Proceedings of the IEEE/CVF International Conference on Computer Vision*, 2021. 6
- [46] K. Simonyan and A. Zisserman, "Very deep convolutional networks for large-scale image recognition," *arXiv preprint arXiv:1409.1556*, 2014. 6
- [47] B. Zhou, A. Lapedriza, A. Khosla, A. Oliva, and A. Torralba, "Places: A 10 million image database for scene recognition," *IEEE Transactions on Pattern Analysis and Machine Intelligence*, 2017. 6
- [48] G. Ou, G. Yu, C. Domeniconi, X. Lu, and X. Zhang, "Multi-label zero-shot learning with graph convolutional networks," *Neural Networks*, vol. 132, pp. 333–341, 2020. 6
- [49] Z. Ji, B. Cui, H. Li, Y.-G. Jiang, T. Xiang, T. Hospedales, and Y. Fu, "Deep ranking for image zero-shot multi-label classification," *IEEE Transactions on Image Processing*, vol. 29, pp. 6549–6560, 2020. 6
- [50] S. Narayan, A. Gupta, S. Khan, F. S. Khan, L. Shao, and M. Shah, "Discriminative region-based multi-label zero-shot learning," in *Proceedings of the IEEE/CVF International Conference on Computer Vision*, 2021, pp. 8731–8740. 7, 8
- [51] J. Deng, W. Dong, R. Socher, L. Li, K. Li, and L. Fei-Fei, "Imagenet: A large-scale hierarchical image database," in *Proceedings of the IEEE/CVF Conference on Computer Vision and Pattern Recognition*, 2009. 8
- [52] G. Tsoumakas and I. Katakis, "Multi-label classification: An overview," *International Journal of Data Warehousing and Mining*, 2007. 8, 9
- [53] Y. Gong, Y. Jia, T. Leung, A. Toshev, and S. Ioffe, "Deep convolutional ranking for multilabel image annotation," *arXiv preprint arXiv:1312.4894*, 2013. 8, 9
- [54] S. Ren, K. He, R. Girshick, and J. Sun, "Faster r-cnn: Towards real-time object detection with region proposal networks," in *Advances in Neural Information Processing Systems*, 2015. 9
- [55] S. Rahman, S. Khan, and N. Barnes, "Polarity loss for zero-shot object detection," *arXiv preprint arXiv:1811.08982*, 2018. 9



Akshita Gupta is a MASc student at University of Guelph and Vector Institute for Artificial Intelligence. Previously, she was a Data Scientist at Bayanat LLC, Abu Dhabi and a Research Engineer at the Inception Institute of Artificial Intelligence. She serves as a reviewer for CVPR, ECCV, ICCV, and TPAMI. She has worked as an Outreachy intern at Mozilla in 2018. Her research interest include low-shot (few-, zero-) classification, semantic/instance segmentation, object detection, and open-world learning.



paper award at ICVGIP 2014. His research interests include computer vision and machine learning.

Sanath Narayan is a Research Scientist at the Technology Innovation Institute, Abu Dhabi. He previously worked as a Research Scientist at Inception Institute of Artificial Intelligence and as a Senior Technical Lead at Mercedes-Benz R&D India. He has served as a program committee member for several premier conferences including CVPR, ICCV and ECCV. He has been recognized as an outstanding/top reviewer multiple times at these conferences. He received his Ph.D. degree from the Indian Institute of Science in 2016. His thesis was awarded the best doctoral symposium



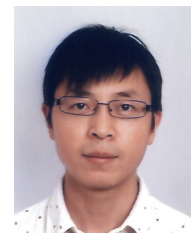
Western Australia in 2016. His thesis received an honorable mention on the Dean's List Award. He has published over 100 papers in high-impact scientific journals and conferences. His research interests include computer vision and machine learning.

Salman Khan is an Associate Professor at MBZ University of Artificial Intelligence. He has been an Adjunct faculty with Australian National University since 2016. He has been awarded the outstanding reviewer award at IEEE CVPR multiple times, won the best paper award at 9th ICPRAM 2020, and won 2nd prize in the NTIRE Image Enhancement Competition alongside CVPR 2019. He served as a (senior) program committee member for several premier conferences including CVPR, ICCV, ICML, ECCV and NeurIPS. He received his Ph.D. degree from The University of



computer vision and machine learning, such as object recognition, object detection, action recognition and visual tracking. He has published more than 100 articles in high-impact computer vision journals and conferences in these areas. He serves as a regular senior program committee member for leading computer vision conferences such as CVPR, ICCV, and ECCV.

Fahad Khan is currently a faculty member at MBZUAI, United Arab Emirates and Linkoping University, Sweden. He received the M.Sc. degree in Intelligent Systems Design from Chalmers University of Technology, Sweden and a Ph.D. degree in Computer Vision from Autonomous University of Barcelona, Spain. He has achieved top ranks on various international challenges (Visual Object Tracking VOT: 1st 2014 and 2018, 2nd 2015, 1st 2016; VOT-TIR: 1st 2015 and 2016; OpenCV Tracking: 1st 2015; 1st PASCAL VOC 2010). His research interests include a wide range of topics within



Ling shao is a Distinguished Professor with the UCAS-Terminus AI Lab, University of Chinese Academy of Sciences, Beijing, China. He was the founding CEO and Chief Scientist of the Inception Institute of Artificial Intelligence, Abu Dhabi, UAE. He was also the Initiator, founding Provost and EVP of MBZUAI. His research interests include generative AI, vision and language, and AI for healthcare. He is a fellow of the IEEE, the IAPR, the BCS and the IET.



Joost van de Weijer received the Ph.D. degree from the University of Amsterdam in 2005. He was a Marie Curie Intra-European Fellow at INRIA Rhone-Alpes, France, and from 2008 to 2012 was a Ramon y Cajal Fellow at the Universitat Autònoma de Barcelona, Spain, where he is currently a Senior Scientist at the Computer Vision Center and leader of the Learning and Machine Perception (LAMP) Team. His main research directions are color in computer vision, continual learning, active learning, and domain adaptation.

APPENDIX**PROPOSED ZSL SPLITS**

Here, we tabulate the unseen classes in the proposed ZSL splits of both datasets: NUS-WIDE [2] and Open Images [34]. While the 84 unseen classes in the new split of NUS-WIDE are given in Tab. 12, the 367 unseen classes of Open Images are given in Tab. 13. Due to the large number of the seen classes in both datasets, they have been listed in our code repository.

TABLE 12
84 unseen classes in the proposed split of the NUS-WIDE dataset

actor	dance	glacier	mountains	protesters	skyscraper	temple
beach	dancing	grass	museum	railroad	snow	tower
book	diving	harbour	night	rainbow	statue	town
buildings	dress	helicopters	nighttime	reflections	storms	trees
canoe	earthquake	human	ocean	river	streets	village
cellphones	fire	hut	outside	road	sun	warehouse
cemetery	firefighter	lakes	park	rocks	sunny	water
city	flags	landscapes	people	running	sunset	waterfalls
cityscape	food	leaves	person	sand	sunshine	wedding
clouds	frost	maps	police	sea	surf	windows
cloudy	gardens	microphones	pool	sky	swimmers	winter
coast	girls	moon	protest	skyline	tattoo	zoo

TABLE 13
367 unseen classes in the proposed split of the Open Images dataset

4 × 100 metres relay	Abseiling	Academic certificate	Acerola	Agaricomycetes
Airbus a330	Akita inu	Amaryllis belladonna	American bulldog	American shorthair
Amphibious assault ship	Amphibious transport dock	Anchor handling tug supply vessel	Apiales	Aquifoliaceae
Aquifoliales	Araneus	Armored cruiser	Asian food	Aubretia
Australian rules football	Australian silky terrier	Auto race	Baker	Balinese
Ballroom dance	Bandy	Barque	Barquentine	Barramundi
Barrel racing	Bass	Basset artésien normand	Beach handball	Bell 412
Bengal	Bentley continental flying spur	Biceps curl	Biewer terrier	Big mac
Birman	Blackbird	Blt	Bmw 3 series (e90)	Bmw 320
Bmw 335	Bmw 5 series	Boa	Bodyguard	Boeing
Boeing 717	Boeing 787 dreamliner	Boeing c-40 clipper	Bombardier challenger 600	Bombycidae
Boston butt	Bouillabaisse	Breckland thyme	Brig	Brigantine
British bulldogs	British semi-longhair	British shorthair	Broholmer	Bruschetta
Bullmastiff	Burmese	Burmilla	Burnet rose	Caesar salad
Calochortus	Camellia sasanqua	Canaan dog	Canard	Canoe slalom
Canoe sprint	Caravel	Caridean shrimp	Carnitas	Carom billiards
Carrack	Catalan sheepdog	Caucasian shepherd dog	Cavapoo	Celesta
Cessna 150	Cessna 172	Cessna 185	Cessna 206	Champignon mushroom
Char kway teow	Charadriiformes	Chassis	Cheesesteak	Chicory
Chinese hawthorn	Churchill tank	Cinclidae	Coccoloba uvifera	Cod
Colias	Colorado blue columbine	Common rudd	Common snapping turtle	Condor
Conformation show	Corn chowder	Crane vessel (floating)	Cross-country skiing	Cuatro
Curtiss p-40 warhawk	Custom car	Czechoslovakian wolfdog	Dame's rocket	Damson
Datura innoxia	Day (Unit of time)	Deep sea fish	Degu	Dirt track racing
Diving	Dobermann	Douglas sbd dauntless	Dragon	Dredging
Drentse patrijshond	Drever	Drilling rig	East siberian laika	Eastern diamondback rattlesnake
Emberizidae	Endurocross	English draughts	Escargot	Estonian hound
Eurasier	European food	European garden spider	European green lizard	Everlasting sweet pea
Exercise	F1 Powerboat Racing	Fast attack craft	Fauna	Fawn lily
Finnish hound	First generation ford mustang	Flatland bmx	Floating production storage and offloading	Flora
Fluyt	Flxible new look bus	Focke-wulf fw 190	Forage fish	Ford model a
Fortepiano	Four o'clock flower	Four o'clocks	Free solo climbing	Freediving
Freestyle swimming	Fried prawn	Frittata	Fudge	Galeas
Galgo español	German pinscher	German spitz	German spitz klein	German spitz mittel
Gladiolus	Go	Grumman f8f bearcat	Gulfstream iii	Gulfstream v
Gumbo	Gumdrop	Gunboat	Gymnast	Ham
Hapkido	Hawthorn	Heavy cruiser	Hula	Hunting
Hydrangea serrata	Hyssopus	Icelandic sheepdog	Icon	Jackup rig
Jaguar mark 1	Jaguar xk150	Japanese Camellia	Japanese rhinoceros beetle	Jamthund
Karelian bear dog	Keelboat	Khinkali	Kishu	Kobe beef
Korat	Kuy teav	Lagotto romagnolo	Laksa	Lamborghini
Lamborghini aventador	Landslide	Large-flowered evening primrose	Light cruiser	Lingonberry
Lissotriton	Longship	Lovebird	Lugger	Mackerel
Maglev	Maidenhair tree	Maine coon	Manchester terrier	Manila galleon
Manx	Matsutake	Mcdonnell douglas dc-9	Mcdonnell douglas f-15e strike eagle	Mcdonnell douglas f-4 phantom ii
Media player	Mercedes-benz e-class	Microvan	Mikoyan mig-29	Milkfish
Milling	Mitsuoka viewt	Motor torpedo boat	Motorcycle speedway	Musk deer
Muskox	Nebelung	Nectar	Negroni	Network interface controller
Newt	Nightingale	Norwegian forest cat	Norwegian lundehund	Nova scotia duck tolling retriever
Obstacle race	Offshore drilling	Oil field	Omelette	Orangery
Ortolan bunting	Patriarch	Patrol boat	Patterdale terrier	Pda
Peccary	Peppers	Perch	Persian	Pilot boat
Pinscher	Piper pa-18	Pit cave	Pixie-bob	Platform supply vessel
Player piano	Polish hunting dog	Polish lowland sheepdog	Pomacentridae	Pontiac chieftain
Porsche 911 gt2	Porsche 911 gt3	Porsche 959	Portuguese water dog	Potato pancake
Pronghorn	Pumi	Quesadilla	Quinceañera	Ragdoll
Rattlesnake	Reefer ship	Republic p-47 thunderbolt	Requiem shark	Research vessel
Rice ball	Rings	Roller hockey	Roller in-line hockey	Rolls-royce phantom
Rolls-royce phantom iii	Rowan	Lugger	Ruf ctr	Russell terrier
Russian blue	Rusty-spotted cat	Saarloos wolfdog	Sailboat racing	Salep
Salisbury steak	Salt-cured meat	Samgyeopsal	Sardine	Savannah
Schisandra	Schnecken	Shenyang j-11	Shiba inu	Shikoku
Ship of the line	Sighthound	Sikorsky s-61	Ski cross	Ski touring
Skyway	Slalom skiing	Slide guitar	Sloppy joe	Smooth newt
Snipe	Snowshoe	Sport climbing	Sport kite	Stabyhoun
Stall	Steak tartare	Submarine chaser	Sukhoi su-27	Sukhoi su-30mkk
Sukhoi su-35bm	Synagogue	Taekyeon	Tamaskan dog	Tapistry
Telemark skiing	Tervuren	Tibetan spaniel	Tiki	Torpedo boat
Toy fox terrier	Toyger	Trout	Tteokbokki	Tufted capuchin
Tvr	Ukulele	Uneven bars	Vienna sausage	Vihuela
Viol	Virginia opossum	Viverridae	Volkswagen golf mk5	Volkswagen type 14a
Volpino italiano	Vought f4u corsair	Wasserfall	Roller in-line hockey	Weed
Western pleasure	White shepherd	World rally championship	Wren	Yarrow
Zwiebelkuchen	Épée			